Pulsed near-infrared photoacoustic spectroscopy of blood

J Laufer*, C Elwell, D Delpy and P Beard,
Department of Medical Physics & Bioengineering, University College London, UK

The aim of this study was to use pulsed near infrared photoacoustic spectroscopy to determine the oxygen saturation (SO_2) of a saline suspension of red blood cells in vitro. The photoacoustic measurements were made in a cuvette which formed part of a larger circuit through which the red blood cell suspension was circulated. Oxygen saturation of the red blood cell suspension was altered between 2-3% to 100% in step increments using a membrane oxygenator and at each increment an independent measurement of oxygen saturation was made using a co-oximeter. An optical parametric oscillator laser system provided nanosecond excitation pulses at a number of wavelengths in the near-infrared spectrum (740-1040nm) which were incident on the cuvette. The resulting acoustic signals were detected using a broadband (15MHz) Fabry-Perot polymer film transducer. The optical transport coefficient and amplitude were determined from the acoustic signals as a function of wavelength. These data were then used to calculate the relative concentrations of oxy- and deoxyhaemoglobin, using their known specific absorption coefficients and an empirically determined wavelength dependence of optical scattering over the wavelength range investigated. From this, the oxygen saturation of the suspension was derived with an accuracy of ±5% compared to the co-oximeter SO_2 measurements.

1. Introduction

When pulsed near-infrared light is incident on biological tissue, it is strongly scattered and eventually absorbed by tissue chromophores such as haemoglobin resulting in thermal expansion. If the optical pulse duration is much shorter than the thermal and stress relaxation times of the tissue, a thermoelastic stress wave is induced which then propagates away from the heated volume. Its amplitude and temporal characteristics contain information on the optical properties of the absorber. In photoacoustic spectroscopy, the wavelength of the excitation laser pulse is varied altering the characteristics of the thermoelastic wave due to the wavelength dependent change in the optical properties of the tissue chromophore. Blood oxygen saturation in particular can be determined from the multi-wavelength absorbance-related measurements extracted from the photoacoustic signals by exploiting the known differences in the absorption spectra of oxy- (HbO_2) and deoxyhaemoglobin (HHb). This principle could be incorporated into photoacoustic imaging, which has been used for mapping the brain of small mammals *in vivo* with high spatial resolution[1] to provide functional as well as structural information.

There have been a number of studies in which photoacoustic spectroscopy, using at least two wavelengths, was applied to the detection of oxygenation induced changes in the optical properties of blood[2,3,4,5]. The studies confirmed that changes in blood oxygenation provide qualitative changes in the photoacoustic attenuation spectrum but did not address the accuracy with which SO_2 can be calculated from the measurements. The objective of the work presented in this paper was to investigate the sensitivity limit of photoacoustically determined blood oxygen saturation. In order to obtain maximum accuracy and precision, all measurements were made *in vitro* by generating photoacoustic waveforms in a cuvette which provided the simplest optical and acoustic detection geometry. In order to quantify the uncertainty in the photoacoustically determined SO_2, all known error sources were incorporated into the calculation. The accuracy of the photoacoustic SO_2 measurements was determined by comparing them to measurements made with a co-oximeter.

Since the detected photoacoustic signal is a direct representation of the absorbed optical energy distribution, two key physical processes need to be considered in order to extract parameters that relate to the optical properties of blood. Firstly, the distribution of absorbed laser energy. This is discussed in sections 2 and 3 in which the optical properties of blood and a simple model of light transport are described. Secondly, the manner in which the absorbed laser energy distribution is encoded on the acoustic wave. This is discussed in section 4. The experimental system is described in section 5 and the methods used to obtain the photoacoustic spectra and recover a measurement of SO_2 from

* Correspondence: J Laufer, Department of Medical Physics & Bioengineering, University College London, 11-20 Capper Street, London WC1E 6JA, UK, e-mail: jlaufer@medphys.ucl.ac.uk,
web: http://www.medphys.ucl.ac.uk/research/borl/

these are described in section 6. In section 7 the experimentally measured photoacoustic spectra and the values of SO_2 obtained are presented.

2. Optical properties of blood

The main components that determine light transport in whole blood are the red blood cells (erythrocytes), the white blood cells and the plasma. The main absorber in blood in the near-infrared wavelength range is haemoglobin in its two oxygenation states of oxy- and deoxyhaemoglobin. Haemoglobin is contained in the red blood cells, which are of discoid shape and are bounded by a cell membrane. The membrane and the intracellular fluid have a slightly higher refractive index than the surrounding plasma. The difference in refractive index causes scattering, which is mainly dependent on the concentration of red blood cells, also described as the haematocrit. The directivity and magnitude of scattering has also been shown to be affected by the salinity of the plasma[6], which can cause shrinking or expanding of the cells. White blood cells do not absorb significantly in the near-infrared but add to the scattering. This can be neglected here, since the blood used in this study was depleted of white blood cells. Plasma contains water and a number of absorbing chromophores, such as bilirubin. In this study, the plasma was removed and replaced with a saline solution. Therefore, the optical attenuation spectrum of the investigated blood samples is defined by the absorption due to HHb, HbO_2, water and scattering from red blood cells as shown in Figure 1.

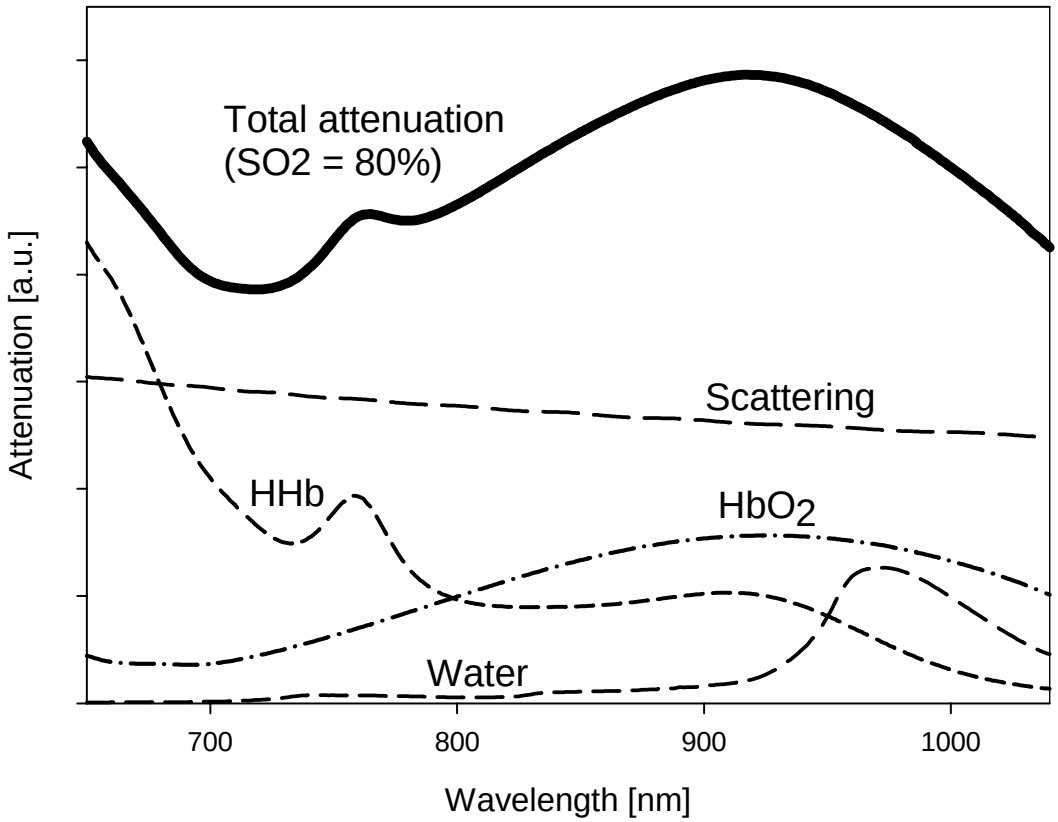

Figure 1 The three main absorbers in a saline blood suspension (HHb, HbO_2 and water) combined with the effects of scattering by red blood cells contribute to the total optical attenuation. An example of the total attenuation calculated for an oxygen saturation of 80% is shown by the thick line.

3. Modelling the light distribution in blood

A simple model was used to describe the light distribution in blood along the axial direction of a collimated excitation beam at normal incidence. It is given by equation (1) below

$$I(z) = I_0 \exp(-\mu_t \, z) \qquad (1)$$

with

$$\mu_t = \mu_a + \mu_s' \qquad (2)$$

where μ_t is the transport coefficient, μ_a is the absorption coefficient, μ_s' is the reduced scattering coefficient, $I(z)$ is the depth dependent fluence distribution and I_0 is the fluence at the surface.

The transport coefficient of blood, defined as the sum of the absorption coefficient and the reduced scattering coefficient, was chosen in preference to the effective attenuation coefficient, μ_{eff}, defined by diffusion theory. Since scattering by red blood cells is generally weaker than absorption and is also highly directional ($g > 0.97$)[6,7], the use of diffusion theory is not strictly valid to describe the propagation of light in blood. The validity of equation (1) was tested by simulating the axial light distribution using a Monte Carlo model for a variety of values of μ_a and μ_s' representative of various physiological haematocrits[6]. An exponential function was then fitted to the modelled data to recover μ_t and this was compared to the known value given by equation (2). Very good agreement between the two values (<1%) was found for combinations where μ_a was equal or greater than μ_s'. As will be confirmed by the results later, this is the predominant situation in blood. If μ_a was smaller than μ_s', the error in the fitted μ_t was typically less than 15%. In this regime, the diffusion approximation may be more appropriate. However, since such combinations of μ_a and μ_s' in blood only occur at a small number of wavelengths at either end of the near-infrared spectrum (750nm > λ >1000nm) depending on the level of oxygen saturation, the effect of this error on the calculated SO_2 was neglected.

4. Thermoelastic signal generation

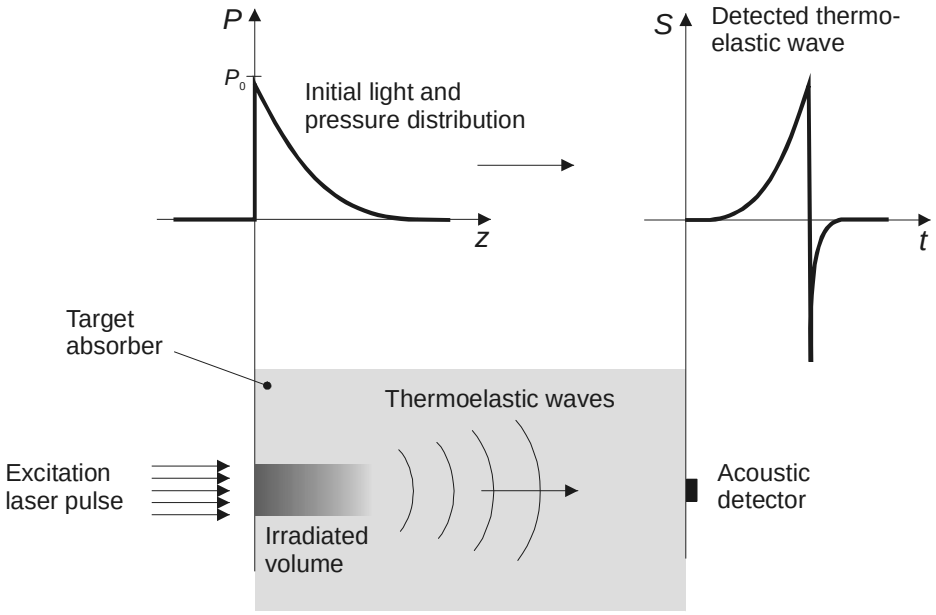

Figure 2 Thermoelastic wave generation in an absorbing medium. The initial compressive part of the detected signal corresponds to the initial stress distribution, which is proportional to the axial distribution of the absorbed energy in the irradiated volume. The positive peak of the signal corresponds to the absorbed energy at the surface of the sample. The negative peak is caused by edge waves from the perimeter of the excitation beam.

The absorption of a short optical pulse in blood causes localised heating and rapid thermal expansion, which generates a thermoelastic stress wave as shown in Figure 2. Assuming stress confinement, the initial pressure distribution can be described by rewriting equation (1) as

$$P(z) = I_0 \, \mu_a \, \Gamma \exp(-\mu_t \, z) \qquad (3)$$

where $P(z)$ is the depth dependent pressure distribution and Γ is the Grüneisen coefficient, which is a measure of the efficiency of the conversion of heat energy to stress. The shape of the initial compressive part of the detected photoacoustic signal is a direct representation of $P(z)$ and can be described by

$$S(t) = K \, P_0 \exp(\mu_t \, c_s \, (t - t_0)) \qquad (4)$$

where K is a constant which describes the sensitivity of the detection system and t_0 is the time difference between the generation of the thermoelastic wave at $t = 0$ and its arrival at the detector. $P_0 = I_0 \, \Gamma \, \mu_a$ and c_s is the speed of sound in water. In this study, equation (4) was fitted to the early arriving compressive part of the photoacoustic signals detected in blood to determine the transport coefficient μ_t.

5. Experimental set-up & methods

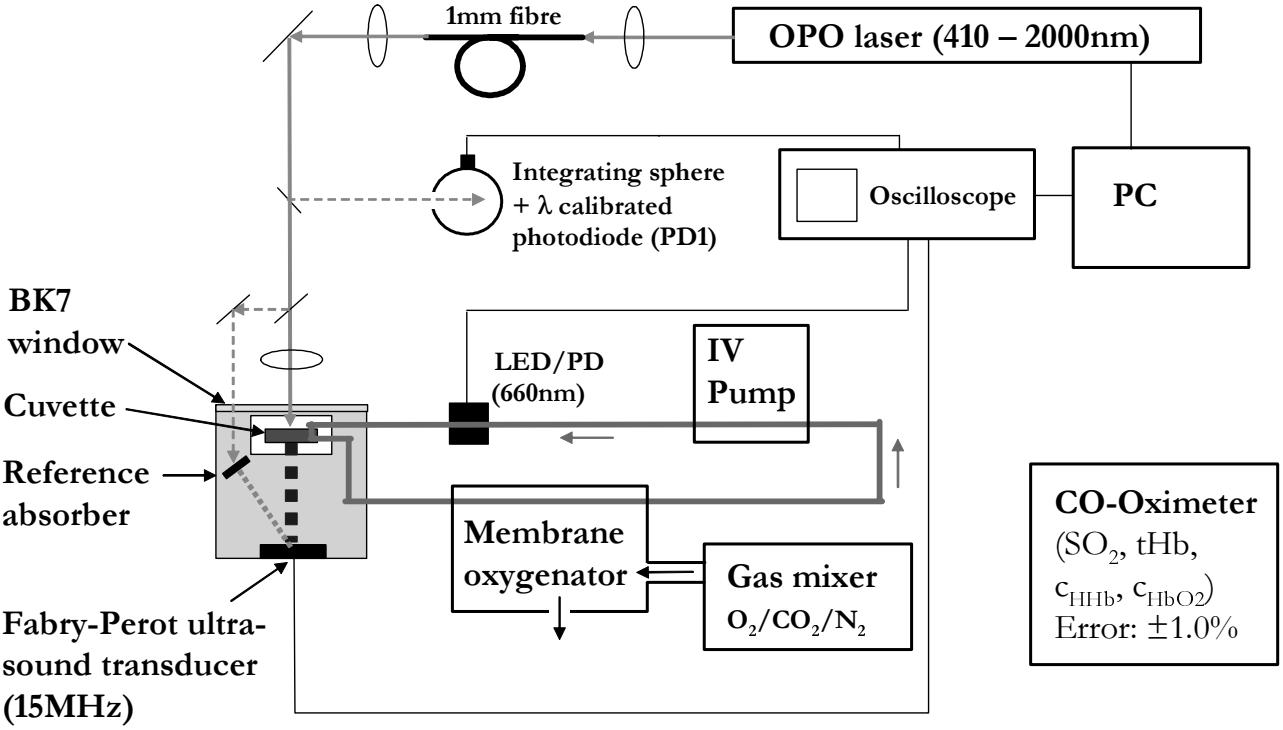

Figure 3 Illustration of the experimental set-up for measuring photoacoustic spectra in blood. The oxygen saturation was varied using a membrane oxygenator. A co-oximeter provided an accurate and independent measurement of oxygen saturation.

Figure 3 shows the experimental set-up. A wavelength tuneable optical parametric oscillator (OPO) laser (VisIR, GWU), pumped by 7ns excitation pulses from a frequency tripled Nd:YAG laser (355nm, Quanta-Ray LAB-170, Spectra-Physics), was used as the excitation source. The output of the OPO laser was coupled into a 1mm fused silica fibre in order to homogenise the beam and to eliminate the effects of lateral beam movement that occurs during OPO wavelength tuning. The output of the fibre was directed onto a cuvette, which was placed in a water bath. The beam diameter incident on the blood was approximately 5mm and the fluence was between 30 and 40 mJ cm^{-2}. The cuvette provided a chamber of 7 mm depth and 12 mm diameter through which blood was pumped continuously. The front window was made of Perspex while the exit window was covered by a 23 μm polymer film in order to minimise

acoustic attenuation. The absorption of the laser pulse generated a thermoelastic wave which propagated through the water bath to an optical ultrasound transducer for detection. The sensing mechanism of this transducer is based upon the detection of acoustically induced changes in the optical thickness of a 75 μm thick Fabry Perot polymer film interferometer and provides a broadband (15 MHz) detection sensitivity of 1.0 kPa[8,9]. A small fraction (8%) of the incident pulse energy was directed to an integrating sphere and detected with a wavelength-calibrated photodiode (PD1). The amplitude of the photodiode output was later used to normalise the photoacoustic waveforms. The photodiode signal and the photoacoustic waveform were averaged over 60 acquisitions and captured using a digital oscilloscope (TDS784D, Tektronix). Four averaged waveforms were captured at each wavelength. Another small fraction of the incident beam was used to generate a photoacoustic signal, which arrived at the transducer after the wave from the cuvette, in a reference absorber. The reference signal was captured at the beginning of each spectral scan and was used to monitor long term drifts in the sensitivity of the Fabry-Perot transducer. The wavelength tuning of the OPO laser and the capture of the photoacoustic waveforms were automated and controlled using LabView. The tuning range was between 740nm and 1040nm in steps of 10nm and the wavelength accuracy was ±0.7nm. An intravenous pump circulated the blood through an extracorporeal membrane oxygenator (Lilliput 1 D901, Dideco) and the cuvette. A gas mixer provided constant air flow through the membrane oxygenator with accurately controlled flow rates of O_2, CO_2 and N_2. Blood oxygen saturation was controlled by adjusting the ratio of O_2 to CO_2 and N_2. A photodiode and an LED (660nm) were placed on opposite sides of a connecting tube in order to measure the changes in transmitted light intensity. This provided a simple means of determining the point of oxygenation equilibrium following a change in the gas mixture. Once equilibrium was reached, a small sample of blood was extracted and analysed with a co-oximeter (IL 482, Instrumentation Laboratories Inc). Co-oximeter measurements were made before and after recording a photoacoustic spectrum. The co-oximeter measured the total haemoglobin concentration (tHb), the concentrations of oxy- and deoxyhaemoglobin and SO_2 with an error of ±1% and therefore provided a highly accurate and independent measurement against which the photoacoustic SO_2 measurements could be compared. The variation in SO_2 before and after a photoacoustic spectral scan was typically less than 1%.

5.1. Sample preparation

Expired blood donations (>30 days) from two subjects were obtained from the blood bank. Heparin (3000 units) was added to approximately 160 ml of blood. The samples were centrifuged at 3000 rpm and the plasma was replaced with a phosphate buffered saline solution (pH 7.4, Sigma Aldrich). Centrifugation and plasma replacement were repeated four times to produce a saline suspension of red blood cells, which was less viscous and of lower protein content than whole blood and extended the lifetime of the membrane oxygenator.

6. Analysis of the photoacoustic spectrum

The waveforms contained in each spectral scan were normalised using the output from the wavelength-calibrated photodiode (PD1) multiplied by a correction factor to compensate for its spectral response. A waveform average with a corresponding standard deviation was calculated from the multiple waveforms that had been captured at each wavelength. Two parameters were extracted from the waveform: a) the peak-to-peak signal amplitude and b) the optical transport coefficient, μ_t, obtained by fitting equation (4) to the waveform as shown in Figure 4. The uncertainty in the two extracted parameters was calculated based on the experimental errors. For the case of the signal amplitude, this was the combination of the standard deviation of the repeated measurements and the standard deviation of the spectral calibration factor of PD1. For the case of the fitted μ_t, its uncertainty was calculated based on the standard deviation of each data point that was contained in the section of the signal to which the exponential function was fitted[10,11]. Large uncertainties in the fitted μ_t, which could have been caused by high levels of noise in the data, would indicate the existence of a wide range of coefficients that could yield an equally good agreement between model and data. In this case, the actual value of the coefficient would not be very significant. Using this analysis, photoacoustic spectra were obtained by two methods. Firstly, the signal amplitude was plotted as a function of excitation wavelength to obtain a relative photoacoustic spectrum. Secondly, by plotting the fitted μ_t as a function of wavelength, a spectrum of the absolute attenuation in blood was obtained. The next section describes how these spectra were used to calculate SO_2.

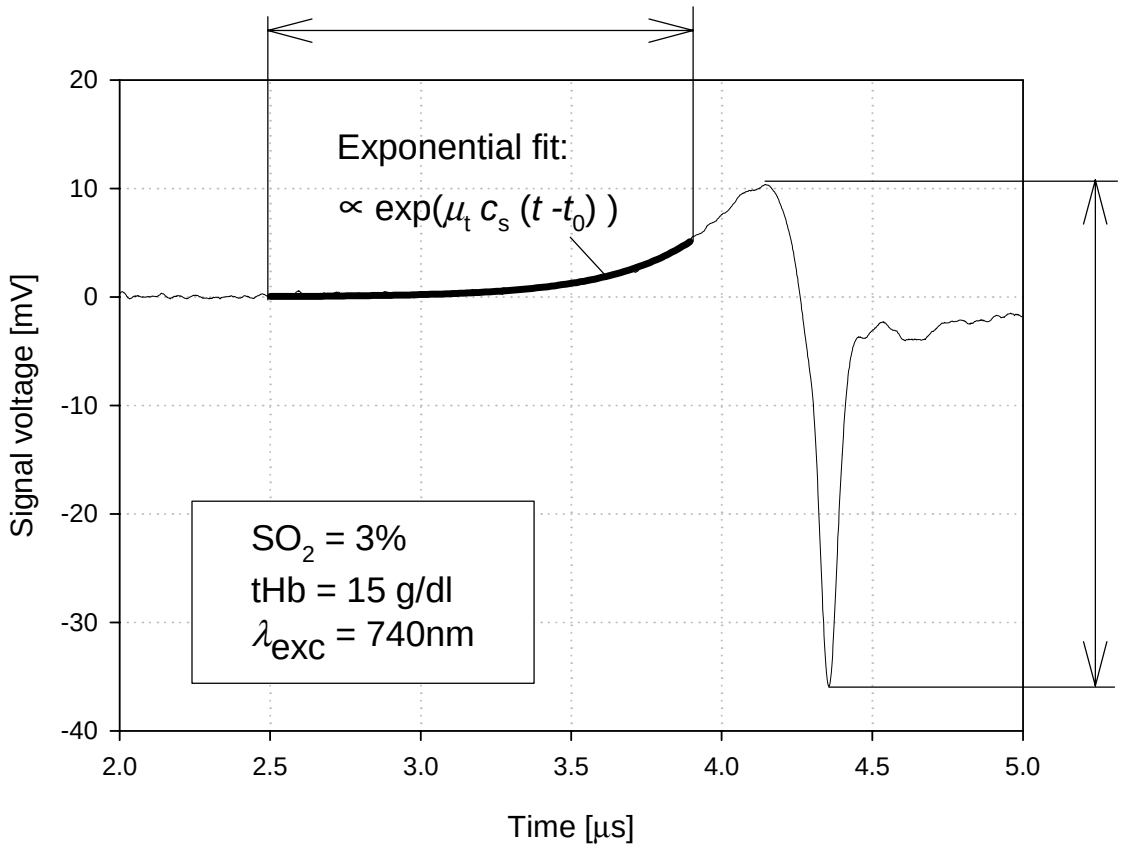

Figure 4 A typical photoacoustic signal detected in deoxygenated blood. Two parameters were extracted from the signal: the peak-to-peak signal amplitude and the optical transport coefficient, μ_t, obtained by fitting an exponential function to the signal as indicated.

6.1. Calculation of blood oxygen saturation

Blood oxygen saturation is defined as the ratio of oxyhaemoglobin concentration, c_{HbO2}, to total haemoglobin concentration as shown below

$$SO_2 = \frac{c_{HbO_2}}{c_{HbO_2} + c_{HHb}} \times 100\% \qquad (5)$$

where c_{HHb} denotes the concentration of deoxyhaemoglobin. The total optical attenuation in blood can be described as follows

$$\mu_t(\lambda) = \mu_{HHb}(\lambda) + \mu_{HbO_2}(\lambda) + \mu_s'(\lambda) + \mu_{a\_water}(\lambda) \qquad (6)$$

where μ_{HHb}, μ_{HbO2}, μ_{a_water} and μ_s' are the absorption coefficients of deoxyhaemoglobin, oxyhaemoglobin, water and the reduced scattering coefficient respectively. In order to calculate c_{HHb} and c_{HbO2} from spectra of the fitted μ_t, equation (6) can be rewritten as

$$\mu_t(\lambda) = \alpha_{HHb}(\lambda)\, c_{HHb} + \alpha_{HbO_2}(\lambda)\, c_{HbO_2} + \alpha_{scat}(\lambda)\, k + \mu_{a\_water}(\lambda) \qquad (7)$$

where $\mu_{HHb}(\lambda)$ is now expressed as the product of the wavelength dependent specific absorption coefficient, $\alpha_{HHb}(\lambda)$, and the concentration, c_{HHb}, of deoxyhaemoglobin. The calculation of $\mu_{HbO2}(\lambda)$ is analogous. The specific absorption coefficients $\alpha_{HHb}(\lambda)$ and $\alpha_{HbO2}(\lambda)$ (units: mm^{-1} mol^{-1}) relate the absorption of the two chromophores to their

concentration and are known very accurately. The contribution of scattering was regarded as equivalent to that of a third chromophore, represented by the product of a wavelength dependent scattering efficiency term, $\alpha_{scat}(\lambda)$, and a scaling factor, *k*, which is proportional to the concentration of erythrocytes. In its simplest approximation, $\alpha_{scat}(\lambda)$ could be regarded as constant. Alternatively, it could be approximated in the form of the reduced scattering coefficient, $\mu_s'(\lambda)$, calculated using Mie theory for a typical erythrocyte size at physiological concentrations. The absorption coefficient of water, μ_{a_water}, in the near-infrared was known and subtracted directly from the fitted μ_t. It is worth pointing out that equations (6) and (7) are only strictly valid for spectral regions where our simple model of light transport (equation (1)) is applicable, i.e. where μ_a is equal or greater than μ_s'.

In order to solve equation (7) with its unknown quantities of c_{HHb}, c_{HbO2} and *k*, a minimum of three measurements at different wavelengths need to be made. In this study, measurements were made at 31 wavelengths between 740nm and 1040nm in order to obtain a full near-infrared spectrum and to achieve good accuracy in the calculation of SO_2. This resulted in 31 simultaneous equations, which were solved using matrix inversion calculations (MatLab). The uncertainties in the amplitude and μ_t spectra were incorporated in the calculations to yield uncertainties in c_{HHb}, c_{HbO2} and hence SO_2.

The detected photoacoustic amplitude spectrum can be described similarly as

$$M_{p-p}(\lambda) = B\left(\alpha_{HHb}(\lambda)\, c_{HHb} + \alpha_{HbO_2}(\lambda)\, c_{HbO_2} + \alpha_{scat}(\lambda)\, k + \mu_{a\_water}(\lambda)\right) \qquad \textbf{(8)}$$

where $M_{p\text{-}p}(\lambda)$ is the measured spectrum of the peak-to-peak signal amplitude and *B* is an unspecified system response factor, which depends on a number of amplitude related parameters such as the laser pulse energy and detector sensitivity. The main difference to equation (5) is the inclusion of the system response as a variable. In this case, a minimum of four measurements at different wavelengths are required to determine c_{HHb}, c_{HbO2}, *k* and *B*.

Before the haemoglobin concentrations could be calculated, it was necessary to correct the spectra of the specific extinction coefficient to take account of the varying linewidth of the OPO laser. Type I OPO lasers show a strong dependence of linewidth not only on emission wavelength but also on pump laser parameters such as pulse duration, beam divergence and beam profile. This can lead to a range in linewidth starting at 2-3nm FWHM at 1000nm to broad emissions of 15-25nm near the so-called degeneracy point at 709nm, which will smear spectral features such as the HHb absorption peak at 760nm. The linewidth spectrum of the OPO was measured and the spectra of the specific extinction coefficient were corrected. This was done by convolving the wavelength dependent linewidth function of the laser source with the known specific absorption spectra of HHb and HbO_2.

7. Results

Figure 5 shows spectra of the measured photoacoustic amplitude, equivalent to $M_{p\text{-}p}(\lambda)$ in equation (8), at different levels of oxygen saturation. It illustrates the gradual change in the spectral attenuation of blood from maximum deoxygenation to complete oxygenation and is in qualitative agreement with the known HHb and HbO_2 spectra. Figure 6 shows spectra of the photoacoustic peak-to-peak amplitude and the fitted μ_t for an oxygen saturation of 3% and the known specific absorption coefficient of HHb. The photoacoustic amplitude spectrum agrees reasonably well with the spectrum of the specific absorption coefficient. However, a comparison of the fitted μ_t spectrum with the specific absorption coefficient spectrum reveals significant differences. Similar differences between the two spectra were found in measurements made at other oxygen saturations. The difference in the μ_t spectra compared to the specific absorption spectrum can be attributed to scattering. The effect of scattering on total attenuation is similar to a dc level that is added to the absorption spectrum, which causes a flattening of absorption peaks as illustrated by the spectrum of the fitted μ_t in Figure 6. In order to incorporate the contribution of scattering into the calculation of SO_2 later, the spectral dependence of scattering, $\alpha_{scat}(\lambda)$, needed to be obtained. To achieve a reasonable approximation of the μ_s' spectrum, Mie theory could have been used. However, since the absorption coefficient of HHb and HbO_2 could be calculated very accurately from the total haemoglobin concentration and oxygen saturation measurement of the co-oximeter, the scattering spectrum was instead obtained by subtracting the calculated μ_{HHb}, μ_{HbO2} and the known μ_{a_water} from the fitted μ_t for all studied SO_2 levels.

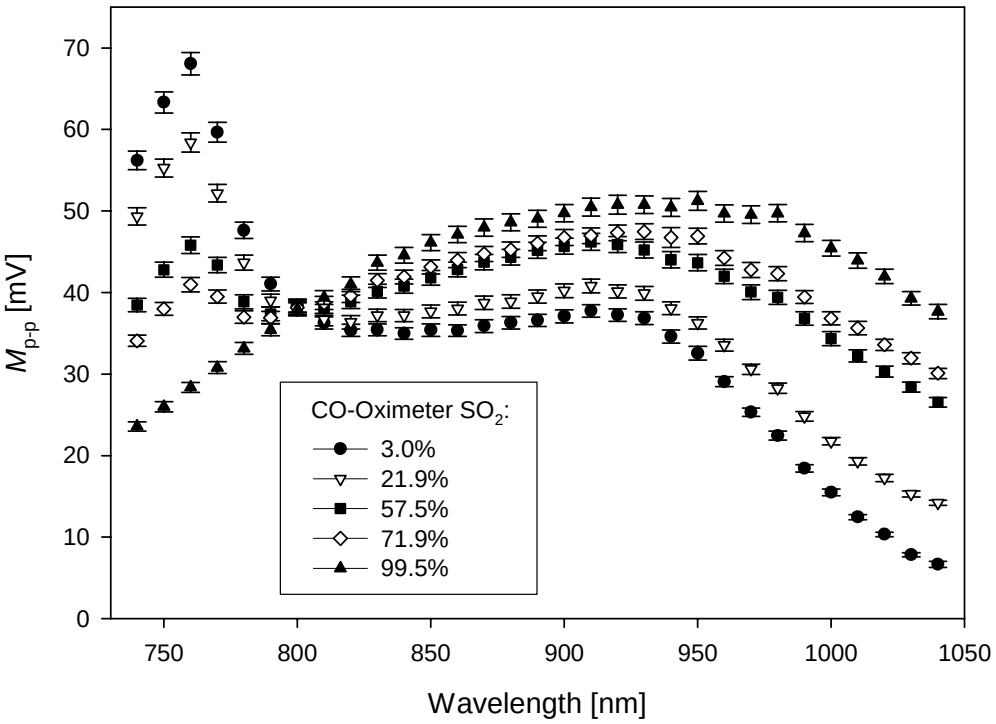

Figure 5 Photoacoustic amplitude spectra of blood for different levels of SO_2.

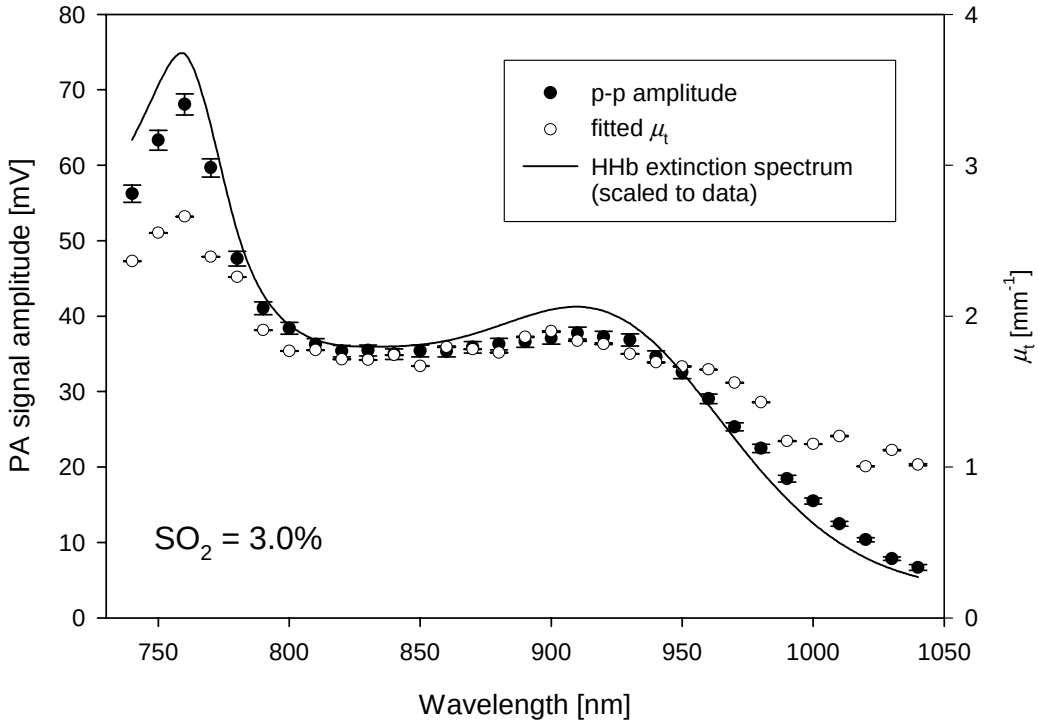

Figure 6 Photoacoustic spectra of the peak-to-peak amplitude, the fitted μ_t and the known specific absorption coefficient of deoxyhaemoglobin. The photoacoustic spectra were measured at an oxygen saturation of 3%.

This analysis was only performed on the μ_t data from one of the two studied blood samples and produced a spectrum of the reduced scattering coefficient as shown in Figure 7. Each data point in Figure 7 represents the average of the μ_s' values calculated for each SO_2 level.

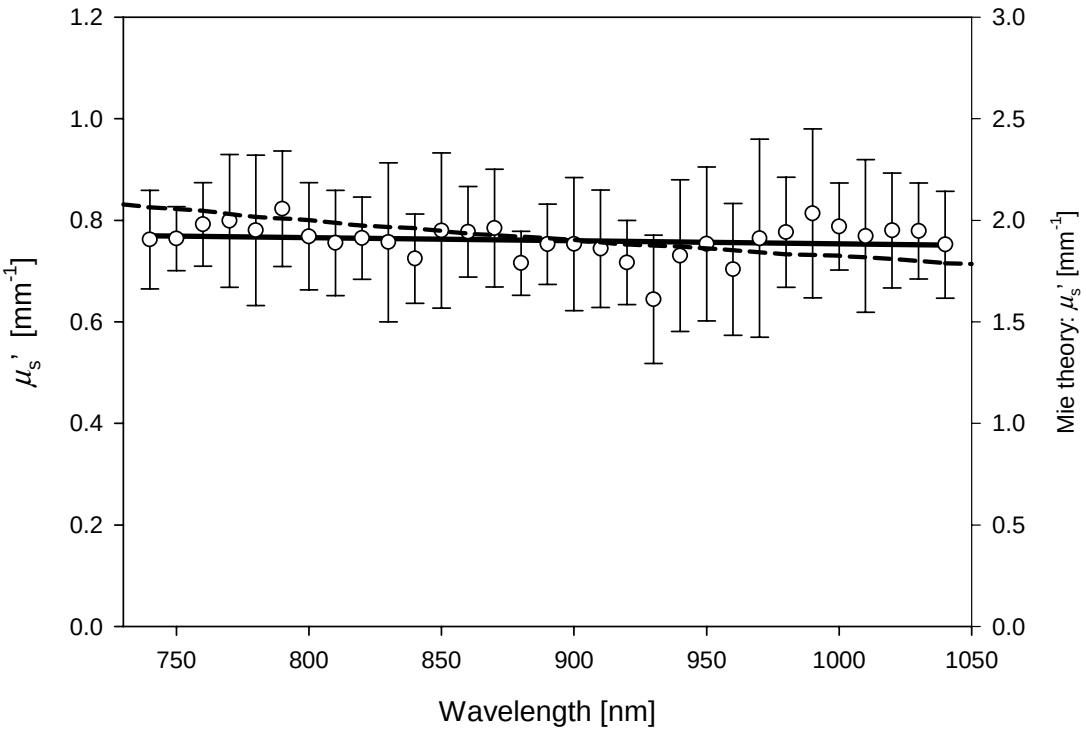

Figure 7 The reduced scattering coefficient of blood (○) calculated from the fitted μ_t data for all oxygen saturation levels across the near-infrared spectrum. The solid line is a linear regression through the data used later to describe $\alpha_{scat}(\lambda)$. The dashed line shows the spectral dependence of the reduced scattering coefficient, μ_s', calculated using Mie theory for a haematocrit of 45%.

A linear regression through the μ_s' spectrum was used to provide the wavelength-dependent scattering efficiency, $\alpha_{scat}(\lambda)$. The μ_s' spectrum shown in Figure 7 was subtracted from the fitted μ_t shown in Figure 6 to obtain the total absorption coefficient of haemoglobin, which in Figure 8 is compared to the corresponding amplitude spectrum and the specific absorption spectrum, showing very good agreement between the $\alpha_{HHb}(\lambda)$ spectrum and the μ_t - μ_s' spectrum. Similar agreement as a result of subtracting μ_s' was found for all other levels of oxygen saturation. The calculated scattering efficiency $\alpha_{scat}(\lambda)$ was later used for the calculation of SO_2 from photoacoustic measurements made on sample 2. This was found to produce more accurate SO_2 values than estimating $\alpha_{scat}(\lambda)$ with Mie theory, which is perhaps not surprising given that its validity is limited to spherical particles. The reasonable agreement of the amplitude data with the specific absorption spectrum of HHb without any corrections to take account of μ_s' also suggests that it is less influenced by scattering than the fitted μ_t. This is because the amplitude part of the waveform originates from regions immediately adjacent to the cuvette window, where the light transport may be dominated by absorption due to the strong forward scattering in blood. By contrast, the compressive part of the photoacoustic waveform, which determines μ_t, originates from photons that have propagated deeper into the cuvette and have undergone more scattering events. For this reason it is necessary to take into account $\mu_s'(\lambda)$ to get good agreement between the fitted μ_t spectrum and the known specific absorption spectrum.

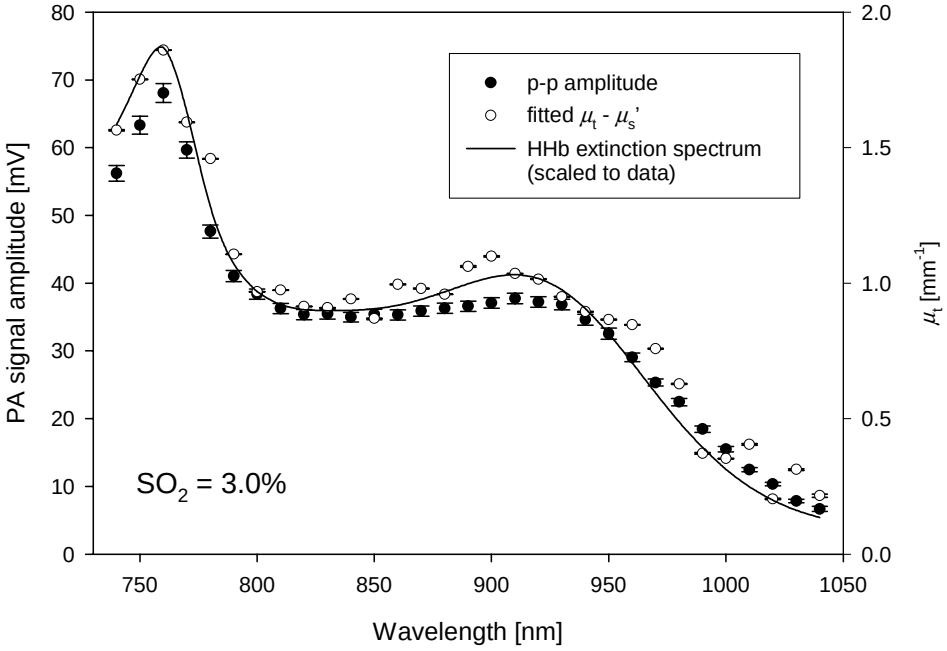

Figure 8 Comparison of the photoacoustic spectra of the peak-to-peak amplitude, the fitted μ_t - μ_s' and the known specific absorption coefficient of deoxyhaemoglobin.

7.1. Photoacoustic SO_2 vs co-oximeter SO_2

The oxygen saturation was calculated from measurements made on blood from sample 2 using the $\alpha_{scat}(\lambda)$ spectrum calculated from blood sample 1 and published spectra of $\alpha_{HHb}(\lambda)$, $\alpha_{HbO2}(\lambda)$ and $\mu_{a\_water}(\lambda)$. In Table 1, co-oximeter readings are compared to the corresponding photoacoustic SO_2 measurements calculated from a selection of measured amplitude and μ_t spectra. Each photoacoustic SO_2 value is given with its associated uncertainty, which is a measure of the level of confidence in the determined SO_2 given the noise in the data and other error sources. The accuracy, which is the difference between the photoacoustically determined SO_2 and the 'gold standard' co-oximeter readings, is given for both amplitude and μ_t based SO_2 measurements.

CO-Oximeter SO_2 [± 1.0%]	Amplitude SO_2 [%]	Accuracy [%] of amplitude SO_2	μ_t based SO_2 [%]	Accuracy [%] of μ_t based SO_2
3.0	-0.7 ± 1.7	-3.7	11.2 ± 0.3	+8.2
21.9	18.0 ± 2.1	-3.9	19.7 ± 0.3	-2.2
51.2	46.2 ± 3.4	-5.0	50.0 ± 0.1	-1.2
57.5	52.2 ± 3.5	-5.5	41.8 ± 0.6	-15.7
71.9	66.3 ± 4.0	-5.6	67.2 ± 0.4	-4.7
99.5	104.7 ± 5.7	+5.2	94.8 ± 0.2	-4.7

Table 1 Comparison of photoacoustically determined SO_2 with independent SO_2 measurements made with the co-oximeter. The accuracy is the difference between the photoacoustically measured SO_2 and the co-oximeter readings.

The photoacoustic SO_2 measurements compare well with the co-oximeter readings and are typically within ±5% for the amplitude data. The μ_t spectra produced an accuracy of typically ±5% with a few outliers of up to 16%. The inaccuracies in the μ_t based SO_2 measurements are possibly due to sporadic low frequency noise on the photoacoustic signals, which translated into noise in the μ_t spectra. Despite these experimental errors, the uncertainties in μ_t based SO_2

are significantly smaller than those of the amplitude measurements, indicating that the precision with which μ_t can be determined from time-resolved measurements is high. This is explained by the use of the curve fitting technique where μ_t was determined from waveforms composed of many data points, which resulted in lower uncertainties than those obtained from only two data points (min, max) for the amplitude measurements.

8. Discussion

This study has shown that, using both the amplitude and time-resolved information contained in photoacoustic waveforms, SO_2 could typically be measured to within ±5% of the co-oximeter reading. Based on the co-oximeter measurements of total haemoglobin concentration and SO_2, a scattering spectrum was calculated suggesting that the contribution of scattering is almost constant in the near-infrared. Using the empirically determined scattering dependence instead of that calculated using Mie theory resulted in improved accuracy in SO_2. However, small discrepancies still exist between photoacoustic and co-oximeter SO_2, which could be due to limitations of the experimental setup and the model of light transport. It was found, for example, that the signal amplitude is very sensitive to small movements in the excitation beam during OPO scanning. This effect was greatly reduced by coupling the beam into an optical fibre. However, despite fibre coupling the OPO output, it was not possible to recover the amplitude spectrum accurately. These differences may be due to changes in the beam profile, which are the result of beam movements during wavelength tuning. This would excite different modes in the fibre and therefore generate a variety of beam profiles, which would affect the signal amplitude in an unpredictable way. The calculation of μ_t spectra of blood also suffered experimental errors due to sporadic low frequency noise, which was probably generated by instabilities in the HeNe laser that interrogates the Fabry-Perot ultrasound transducer. Low frequency noise was found to affect the exponential slope of the photoacoustic signal and hence the fitted μ_t.

The simple model of light transport, which essentially treats absorption and scattering as the sum of two exponential decay constants, allowed the calculation of reasonably accurate SO_2 values compared to the co-oximeter measurements. However, some of the inaccuracies in SO_2 may be due to the limitations in our model describing the light distribution at wavelengths where μ_a is smaller than μ_s'. At those wavelengths, diffusion theory could be a more accurate alternative. One could perhaps envisage the use of a different model of light transport for each wavelength across the spectrum depending on the varying ratio of μ_a and μ_s'. To complicate matters further, blood can also not be regarded as an optically homogeneous medium. When blood flows through blood vessels, a thin layer of plasma is created between the erythrocytes and the vessel wall which reduces friction. A similar effect may be present in the cuvette, which would produce gradually increasing erythrocyte concentrations near the cuvette window and hence gradually increasing μ_a and μ_s' with depth, which is different to the assumed step increase in μ_a and μ_s'. The current model may have to be refined to take account of this. However, since the source of the discrepancy between photoacoustic and co-oximeter SO_2 measurements could be related entirely to the systematic errors in the experimental technique, the current model may turn out to provide a simple yet sufficiently accurate description of the axial light distribution in blood. Most of the above problems can readily be solved, which will allow SO_2 to be determined much more accurately from cuvette-based photoacoustic measurements in future measurements. With further improvements to the experimental setup and analysis, it should in principle be possible to achieve an accuracy comparable to that of the co-oximeter.

9. References

[1] X Wang, Y Pang, G Ku, X Xie, G Stoica,, L Wang, "Noninvasive laser-induced photoacoustic tomography for structural and functional in vivo imaging of the brain," *Nature Biotechnology*, **21(7)**, 803-806 (2003)

[2] R Fainchtein, B Stoyanov, J Murphy, D Wilson, D Hanley, "Local determination of haemoglobin concentration and degree of oxygenation in tissue by pulsed photoacoustic spectroscopy," Proc. SPIE, **3916**, 19-33 (2000)

[3] E Svateeva, A Karabutov, S Solomatin, A Oraevsky, "Optical properties of blood at various levels of oxygenation studied by time resolved detection of laser-induced pressure profiles," *Proc SPIE*, **4618**, 63-75 (2002)

[4] R Esenaliev, I Larina, K Larin, D Deyo, M Motamedi, D Prough, "Optoacoustic technique for non-invasive monitoring of blood oxygenation: a feasibility study," *Appl. Opt.*, **41(22)**, 4722-4731 (2002)

[5] G Paltauf, K Köstli, D Frauchinger, M Frenz, "Spectral optoacoustic imaging using a scanning transducer," *Proc SPIE*, **4434**, 81-88 (2001)
[6] A Roggan, M Friebel, K Doerschel, A Hahn, G Mueller, "Optical properties of circulating human blood in the wavelength range 400-2500nm," *J Biomed Opt*, **4(1)**, 36-46 (1999)
[7] M Hammer, A Yaroslawsy, D Schweitzer, "A scattering phase function for blood with physiological haematocrit," *Physics in Medicine and Biology*, **46**, N65-N69 (2001)
[8] PC Beard, "Interrogation of free-space Fabry-Perot sensing interferometers by angle tuning," *Measurement Science and Technology*, **14**, 1998-2005 (2003)
[9] PC Beard, F Pérennès, TN Mills, "Transduction mechanisms of the Fabry-Perot polymer film sensing concept for wideband ultrasound detection," *IEEE Transactions on Ultrasonics, Ferroelectrics, and Frequency Control*, **46(6)**, 1575-1582 (1999)
[10] JV Beck, KJ Arnold, *Parameter Estimation in Engineering and Science*, John Wiley & Sons, New York (1977)
[11] JG Laufer, PC Beard, SP Walker, TN Mills, "Photothermal determination of optical coefficients of tissue phantoms using an optical fibre probe," *Physics in Medicine and Biology*, **46**, 2515-2530 (2001)